IEEE Photonics Journal
An IEEE Photonics Society Publication

Experiments With Three-Dimensional Integral Imaging Under Low Light Levels

Volume 4, Number 4, August 2012

Adrian Stern
Doron Aloni
Bahram Javidi

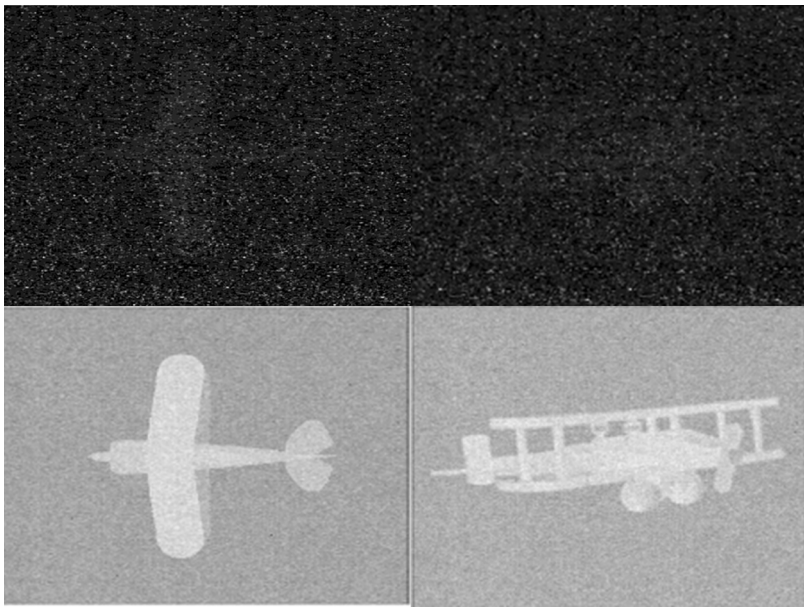

DOI: 10.1109/JPHOT.2012.2205912
1943-0655/$31.00 ©2012 IEEE

IEEE photonics SOCIETY

IEEE

Experiments With Three-Dimensional Integral Imaging Under Low Light Levels

Adrian Stern,[1] **Doron Aloni,**[1] **and Bahram Javidi**[2]

[1]Electro Optical Engineering, Ben-Gurion University of the Negev, Beer-Sheva 84105, Israel
[2]Department of Electrical and Computer Engineering, University of Connecticut, Storrs, CT 06269-2157, USA

DOI: 10.1109/JPHOT.2012.2205912
1943-0655/$31.00 ©2012 IEEE

Manuscript received June 14, 2012; accepted June 20, 2012. Date of publication June 28, 2012; date of current version July 12, 2012. Corresponding author: A. Stern (e-mail: stern@bgu.ac.il).

Abstract: We experimentally demonstrate the possibility of reconstructing 3-D scenes using integral imaging from very photon-starved scenes. It is shown that by using an iterative reconstruction algorithm, it is possible to reconstruct 3-D objects captured with an optical signal just above the CCD image sensors' noise level. Three-dimensional scene reconstruction with integral images with only a few photons per pixel of the image sensor is demonstrated. Optical experimental results are presented.

Index Terms: Image reconstruction, integral imaging, 3-D imaging.

1. Introduction

Integral imaging [1]–[24] is a passive 3-D imaging technique with continuous view point based on the concept of integral photography introduced more than a century ago by G. Lippmann [10]. With integral imaging, multiple views of a 3-D object are captured with an array of apertures, typically implemented by means of a lenslet array or an array of cameras. Each aperture generates a specific view image referred to as an elemental image, and the entire set of elemental images captured is referred to as an integral image. The integral imaging process is described in Section 2.1.

The integral imaging acquisition process is shown in Fig. 1(a). The capturing process may be viewed as a multichannel acquisition process, where each channel generates an elemental image. As such, there is a large redundancy in the captured data permitting various tasks besides basic 3-D visualization, such as imaging through occlusion [11]–[13], 3-D object recognition [1], and 3-D data extraction with very few photons in the scene [14]–[20]. Several works have recently demonstrated that 3-D image visualization [15], [20] and 3-D target recognition [14], [17]–[19], [21] are theoretically possible from extremely low number of photons captured with integral imaging, which can be implemented using photon-counting detectors. However, photon-counting image sensors, in general, are very expensive and may be available with only a limited number of pixels. Therefore, in this paper, we address a more robust case; that is, the reconstruction of 3-D objects captured with integral imaging using conventional (CCD or CMOS) sensors under very low light conditions. We investigate the ability to reconstruct computationally 3-D objects in photon-starved conditions, that is, with irradiance impinging the CCD sensors that is only slightly above the noise levels. Due to the inherent noise of the CCD and CMOS cameras, a larger photon flux is necessary; however, we show that it is possible to reconstruct 3-D images form elemental images with a signal-to-noise ratio (SNR) much lower than 1 by applying appropriate iterative reconstruction algorithms to estimate the original data.

The paper is organized as follows. In Section 2.1, we give a short description of the integral imaging process together with the conventional model used for reconstruction of 3-D images from integral

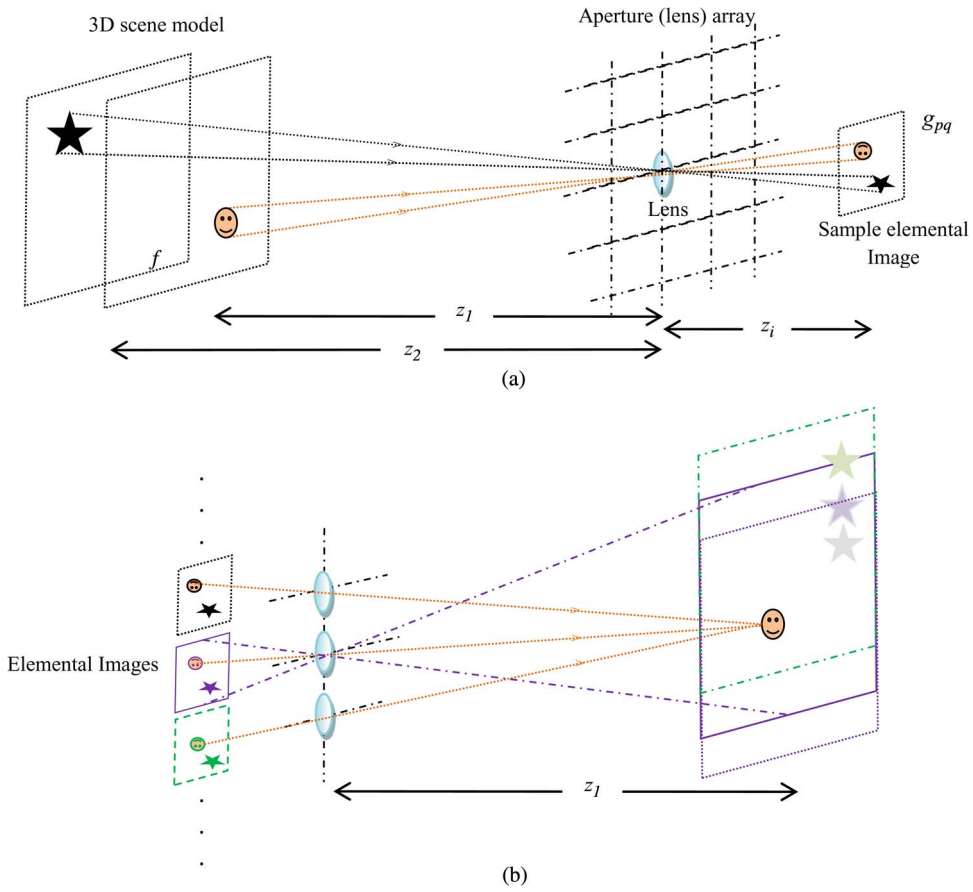

Fig. 1. Schematic of integral imaging setup. (a) Integral imaging scene acquisition. (b) Optical or conventional computational reconstruction. Three sample elemental images from a column of the integral image are shown together with their back projection to plane located at depth z_1.

images captured with regular illumination. Next, in Section 2.2, we present the reconstruction algorithm used for visualization of 3-D images from photon-starved integral images. In Section 3, we show simulation and real optical experimental results. Finally, we conclude in Section 4.

2. Computational Integral Imaging Reconstruction

2.1. Computational 3-D Image Reconstruction by Back Projection

The 3-D imaging process with integral imaging is depicted in Fig. 1. Fig. 1(a) shows the image capturing process. Each aperture, located at node (p, q) of a rectangular grid, captures an elemental image. The reconstruction can be performed optically or computationally [1]. The common computational reconstruction method is by digitally inverse mapping the elemental images [see Fig. 1(b)]. Technically, this is a straightforward process involving summation of the back projections of each elemental image and normalization according to the number of elemental images contributing to each reconstructed voxel. Note that the back projections depend on the lateral magnification $M = -(z_i/z_o)$; thus, it must take into account the reconstructed object plane z_o. Hence, by means of controlling M, the reconstruction can be focused at different object planes (different ranges in the scene). For instance, in Fig. 1(b), the reconstruction is focused on plane z_1. This approach has been used in previous works (see for example [15], [22], and [23]) yielding satisfactory results for integral images captured with regular illumination conditions. Here, we

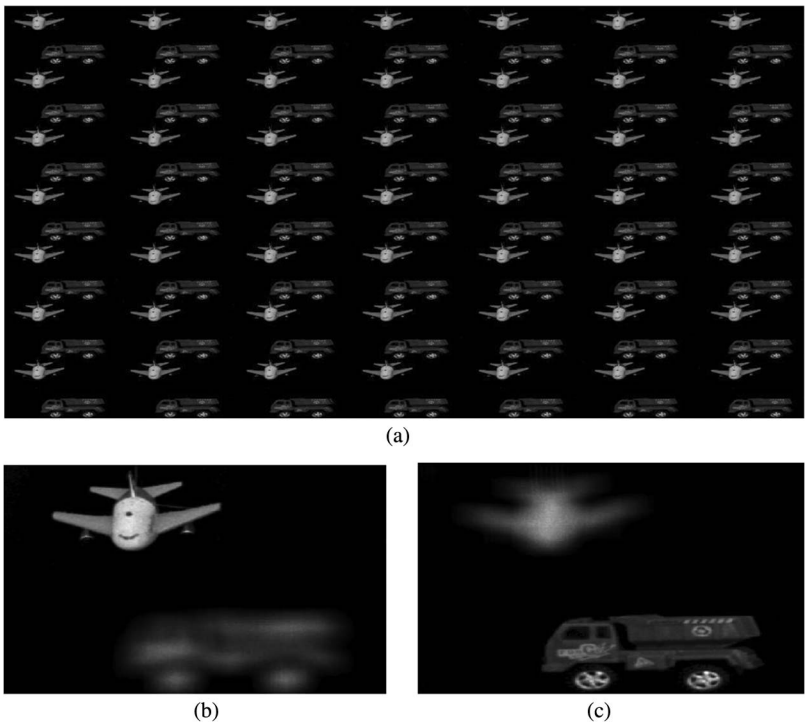

Fig. 2. (a) Integral image consisting of 7 × 7 elemental images captured with large photon flux illumination. Reconstruction of the object planes at distances (z_1) of 50 cm in (b) and 70 cm in (c).

address the problem of computational reconstruction of integral images captured under extremely low illumination in the scene, which requires applying more sophisticated reconstruction algorithms.

In the following, we shall adopt an operator formalism to describe the imaging and back-projection process [20]. The imaging process in Fig. 1(a) can be described with an operator formalism as $\boldsymbol{g} = \mathbf{H}\boldsymbol{f}$, where $\mathbf{H}$ is the forward propagation operator, and $\boldsymbol{f}$ and $\boldsymbol{g}$ are vectors describing the object and the image plane pixels in a lexicographic order, respectively. Technically, the operator $\mathbf{H}$ can be implemented as a matrix or as a function handle (procedure) that maps each pixel from the object plane to the image plane. The back-projection operator is simply the adjoint operator, $\mathbf{H}^{\mathrm{T}}$, so the conventional inverse mapping method can be formulated as applying $\mathbf{H}^{\mathrm{T}}$ on the captured integral images; $\boldsymbol{f}^{\mathrm{bp}} = \mathbf{H}^{\mathrm{T}}\boldsymbol{g}$, where the superscript "bp" stands for back projection.

In one example, the input scene $\boldsymbol{g}$ is shown in Fig. 2(a). The integral image was captured by placing a camera at the nodes of a 7 × 7 array with horizontal and vertical pitch size of 50 mm. We used a 16-bit cooled camera (DTA model DX-1600E). As objects, we used a toy truck located approximately 50 cm from the camera plane and an airplane that was at a distance of approximately 70 cm. Fig. 2(b) and (c) shows examples of reconstruction of two planes of the scene by conventional back projections $\boldsymbol{f}^{\mathrm{bp}} = \mathbf{H}^{\mathrm{T}}\boldsymbol{g}$ from the integral image.

2.2. Computational Integral Imaging 3-D Image Reconstruction of a Scene Captured in Extremely Low Illumination Conditions

In the case of integral images captured with very low input scene SNR considered here, the acquisition process can be modeled by

$$\boldsymbol{g} = \mathbf{H}\boldsymbol{f} + \mathbf{n}, \tag{1}$$

where $\mathbf{n}$ is the acquisition noise and has an intensity much larger than that of the signal. Such an acquisition model is extremely ill conditioned; therefore, conventional back projection, that is $\boldsymbol{f}^{\mathrm{bp}} = \mathbf{H}\boldsymbol{g}$, cannot give good results. In order to handle this problem, we use an iterative reconstruction

algorithm designed for the statistical model of the acquisition process and that incorporates efficiently priors about the object. Iterative algorithms were used previously for computation integral image reconstruction in [20] and [24]. In [24], a sparsity-promoting reconstruction algorithm is used to increase the resolution and decrease superposition artifacts. This kind of algorithms were found to be very effective in compressive imaging for space-bandwidth extension [25] and for 3-D holography [26]; however, their performance is limited when applied to images with very poor SNR [27]. Here, we use the penalized maximum-likelihood expectation maximization (PMLEM) reconstruction algorithm, which we found very effective in our previous study [20]. The PMLEM iteration step is given by

$$\hat{f}^{(k+1)} = \frac{\hat{f}^{(k)}}{\mathbf{s} + \beta \cdot \mathbf{P}\hat{f}^{(k)}} \cdot \mathbf{H}^{\mathbf{T}} \cdot \frac{\mathbf{g}}{\mathbf{H} \cdot \hat{f}^{(k)}}, \tag{2}$$

where $\boldsymbol{g}$ is a lexicographic vector representing the elemental images data, $\hat{f}^{(k)}$ is the reconstructed image vector at k'th iteration, $\mathbf{H}$ is the forward operator that represents the forward projection, $\mathbf{H}^{\mathrm{T}}$ represents the backward projection, and $\mathbf{s}$ is the sensitivity vector with elements $s_j = \sum_{i=1}^{m} h_{i,j}$, $j = 1, \ldots n$, where $h_{i,j}$ is the i, j'th element of the matrix $\mathbf{H}$, accounting for the number of elemental images contributing to reconstruction of the point. $\mathbf{P}$ is the penalty operator, and β is a constant controlling the amount of regularization. The division in (2) should be taken as Hadamard division (component-wise division). Without any penalty, i.e., with $\beta = 0$, the PMLEM algorithm (2) reduces to maximum-likelihood expectation maximization or to Richardson–Lucy algorithm, which are well known for their efficiency in other photon-starved imaging modalities (e.g., [28]–[30]). The penalty $\mathbf{P}$ operator regularizes the reconstruction, thus improves the robustness. Here, we use the total-variation (TV) penalty, which was found in [20] significantly outperforming other penalties. The TV penalty for PMLEM is given by [31]

$$\mathbf{P}\hat{f}_{i,j}^{(k)} = \mathbf{P}\left\{\hat{f}^{(k)}[i,j]\right\} = \frac{\hat{f}^{(k)}[i,j] - \hat{f}^{(k)}[i-1,j]}{u[i-1,j]} + \frac{\hat{f}^{(k)}[i,j] - \hat{f}^{(k)}[i,j-1]}{u[i,j-1]} - \frac{\hat{f}^{(k)}[i+1,j] + \hat{f}^{(k)}[i,j+1] - 2\hat{f}^{(k)}[i,j]}{u[i,j]}, \tag{3}$$

where

$$u(i,j) = \sqrt{\left(\hat{f}^{(k)}[i+1,j] - \hat{f}^{(k)}[i,j]\right)^2 + \left(\hat{f}^{(k)}[i,j+1] - \hat{f}^{(k)}[i,j]\right)^2 + \varepsilon}.$$

The parameter ε is an artificial parameter used to ensure convergence, typically chosen to be less than 1% [31].

3. Experimental Results

The ability to reconstruct 3-D images in photon-starved conditions is experimentally demonstrated here. We repeated the experiment described in Section 2.1 [used for generating the integral image shown in Fig. 2(a)] under extremely low light illumination conditions. The exposure time was set to $t_e = 0.1$ s. Fig. 3(a) shows an example of a captured elemental image. Fig. 3(c) and (d) shows the reconstruction of the two objects located at the two different planes shown in Fig. 2(b) and (c). The reconstruction was carried out with the TV-PLMEM algorithm in (2) with $\beta = 0.25$. It can be seen that owing to the availability of multiple perspectives provided by the multiple elemental images, the objects reconstructed at different depths planes can be visualized despite being completely invisible in the original elemental images [see Fig. 3(a)].

For evaluation of the SNR in the captured integral image, we captured another integral image with the objects removed and the scene in absolute dark conditions. Fig. 3(b) shows an example of such a reference elemental image. We evaluate the SNR in the captured elemental image in

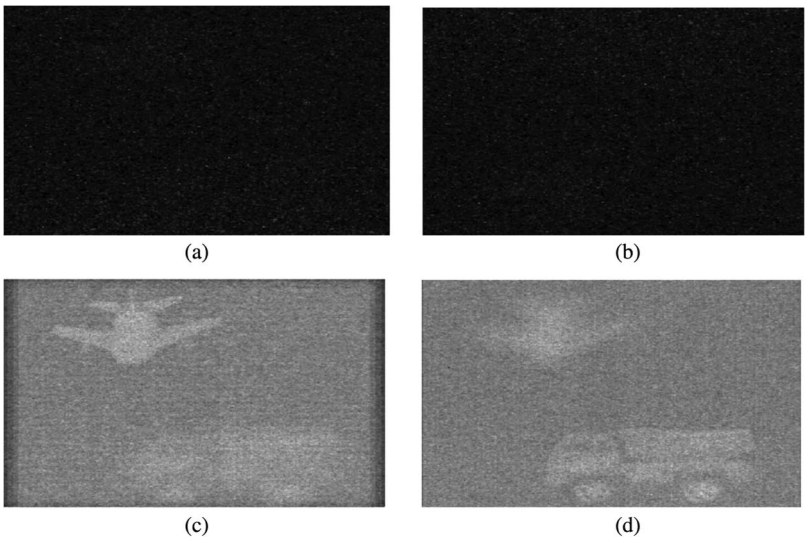

Fig. 3. (a) Elemental images with SNR = 0.16. (b) Elemental image of a low light level scene without objects used as reference for noise calibration, (c,d) TV-MLEM reconstruction of the object planes at distances of 50 cm in (c) and 70 cm in (d).

Fig. 3(a) by:

$$\text{SNR} = \sqrt{\frac{\langle g_o^2 \rangle - \langle n^2 \rangle}{\langle n^2 \rangle}} \tag{4}$$

where $\langle n^2 \rangle$ is the average power of the reference noise image [see Fig. 3(b)]. $\langle g_o^2 \rangle$ is the average power of the object region in the elemental image shown in Fig. 3(a), that is, excluding the dark background area. The segmentation of the object area was done with the help of the high-quality integral image shown in Fig. 2(a) to obtain the region of the support of the object. The SNR in the elemental image shown in Fig. 3(a) was found to be 0.16. Hence, Fig. 3(c) and (d) demonstrates reconstructions from an elemental image array with an SNR significantly below unity.

Equation (4) holds valid since, as we will explain in the following, the dominant noise source is the CCD read noise, which is additive and signal independent. In general, the noise in the CCD image can be expressed as the contribution of the photon noise, dark noise, and read noise:

$$\sqrt{\langle n^2 \rangle} = \sqrt{(\Phi_o + \Phi_b)\eta t_e + D t_e + n_r^2} \tag{5}$$

where Φ_o and Φ_b are object and background incident power (flux), respectively; η is the quantum efficiency; t_e is the exposure time; D is the dark current value; and n_r^2 represents the read noise. By comparing the reference elemental images (scene without objects) in Fig. 3(b) to another image taken with the camera aperture covered, we found that the background noise, $\Phi_b \eta t_e$, is negligible. From the calibration sheet of our camera, we find that $D = 0.2$ electrons/pixel/sec, $\eta = 0.5$ electrons/photons, and $n_r^2 = 12$ electrons rms/pixel. Thus, for the exposure time of $t_e = 0.1$ s and low input SNR, we see that the dominant contribution to the noise in (5) is that of the read noise n_r^2. In this case, the SNR can be approximated as:

$$\text{SNR} \approx \frac{\Phi_o \eta t_e}{\sqrt{n_r^2}}. \tag{6}$$

From (6), we may estimate the number of object photons captured per pixel in Fig. 3(a); that is, $\Phi t_e \approx \text{SNR} \cdot \sqrt{n_r^2}/\eta = 3.8$ photons per pixel.

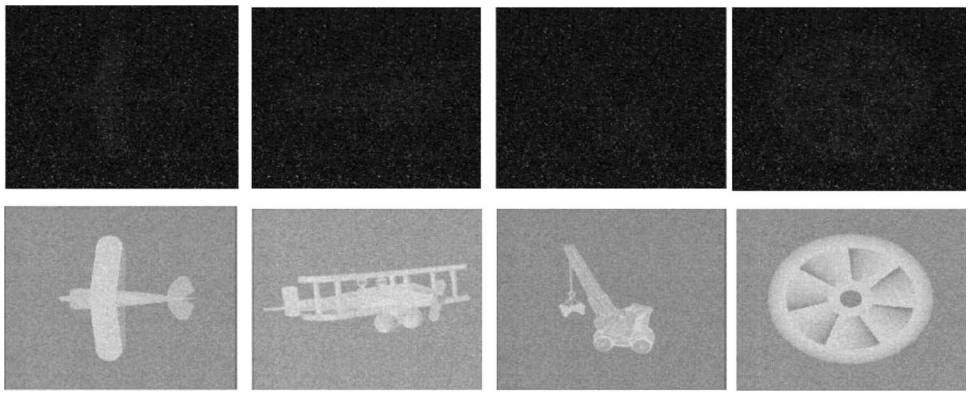

Fig. 4. Upper row: Representative elemental image of the objects used in the simulations (SNR $= 0.21$). Lower row: Reconstructed images with TV-MLEM algorithm.

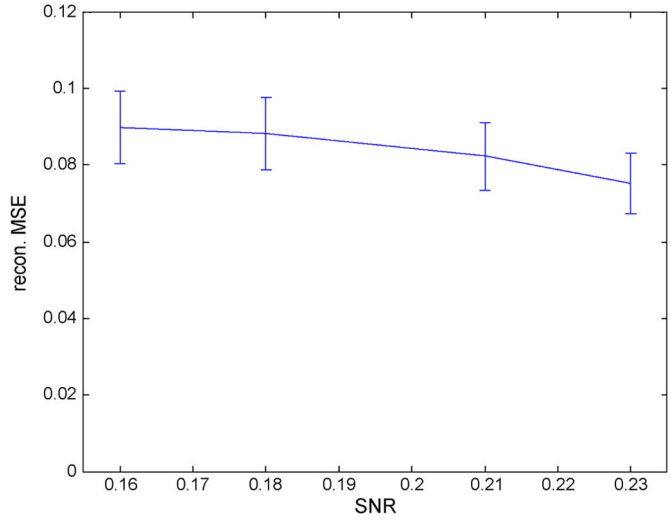

Fig. 5. MSE of reconstructed images as a function of the SNR of the simulated photon-starved integral images.

In order to investigate quantitatively the performance of integral imaging in severe photon-starved conditions, we applied the algorithm in (2) on a set of simulated integral images. By doing so, we can calculate the mean square error between the original image and the reconstructed image. We generated integral images of four different objects at imaging conditions close to that of the real experiment. Elemental images were simulated with SNRs of 0.16, 0.18, 0.21, and 0.23. Representative elemental images and their reconstruction are shown in the upper and lower rows of Fig. 4, respectively.

Fig. 5 shows the decrease of the reconstructed MSE as a function of the integral image SNR. It can be seen that despite some diversity in the MSE, due to the different intensity distributions of the four objects, the general behavior is consistent. For demonstrating the effectiveness of the TV-MLEM, as found in [20], we have reconstructed the integral images also with the maximum-likelihood estimation (MLE) algorithm [15]. We found that the reconstruction peak signal-to-noise ratio (PSNR) obtained with the TV-MLEM algorithm is higher with 2.2 ± 0.4 dB than those with MLE, which is consistent with the finding in [20].

4. Conclusion

We have considered reconstruction of 3-D objects under very low light illumination levels with integral imaging. In the experiments, the irradiance of the scene impinging the CCD image sensor is only slightly above the noise levels. Three-dimensional reconstruction is implemented with integral imaging with only a few photons per pixel of the image sensor. Under these conditions, we applied the TV-MLEM algorithm to reconstruct the 3-D images from captured elemental images with very low SNR. We demonstrated by experiments that we were able to reconstruct and visualize objects located at different planes under photon-starved conditions.

References

[1] A. Stern and B. Javidi, "Three-dimensional image sensing, visualization, and processing using integral imaging," *Proc. IEEE*, vol. 94, no. 3, pp. 591–607, Mar. 2006.

[2] C. Burckhardt, "Optimum parameters and resolution limitation of integral photography," *JOSA*, vol. 58, no. 1, pp. 71–74, Jan. 1968.

[3] Y. Igarashi, H. Murata, and M. Ueda, "3-D display system using a computer generated integral photograph," *Jpn. J. Appl. Phys.*, vol. 17, no. 9, p. 1683, Sep. 1978.

[4] L. Yang, M. McCormick, and N. Davies, "Discussion of the optics of a new 3-D imaging system," *Appl. Opt.*, vol. 27, no. 21, pp. 4529–4534, Nov. 1988.

[5] S. Manolache, A. Aggoun, M. McCormick, N. Davies, and S. Kung, "Analytical model of a three-dimensional integral image recording system that uses circular-and hexagonal-based spherical surface microlenses," *JOSA A*, vol. 18, no. 8, pp. 1814–1821, Aug. 2001.

[6] M. Martínez-Corral, B. Javidi, R. Martínez-Cuenca, and G. Saavedra, "Integral imaging with improved depth of field by use of amplitude-modulated microlens arrays," *Appl. Opt.*, vol. 43, no. 31, pp. 5806–5813, Nov. 2004.

[7] F. Okano, J. Arai, K. Mitani, and M. Okui, "Real-time integral imaging based on extremely high resolution video system," *Proc. IEEE*, vol. 94, no. 3, pp. 490–501, Mar. 2006.

[8] R. Martínez-Cuenca, H. Navarro, G. Saavedra, B. Javidi, and M. Martinez-Corral, "Enhanced viewing-angle integral imaging by multiple-axis telecentric relay system," *Opt. Exp.*, vol. 15, no. 24, pp. 16 255–16 260, Nov. 2007.

[9] H. Liao, N. Hata, S. Nakajima, M. Iwahara, I. Sakuma, and T. Dohi, "Surgical navigation by autostereoscopic image overlay of integral videography," *IEEE Trans. Inf. Technol. Biomed.*, vol. 8, no. 2, pp. 114–121, Jun. 2004.

[10] G. Lippmann, "Epreuves reversibles donnant la sensation du relief," *J. Phys.*, vol. 7, no. 1, pp. 821–825, 1908.

[11] S. H. Hong and B. Javidi, "Three-dimensional visualization of partially occluded objects using integral imaging," *J. Display Technol.*, vol. 1, no. 2, pp. 354–359, Dec. 2005.

[12] B. Javidi, R. Ponce-Díaz, and S. H. Hong, "Three-dimensional recognition of occluded objects by using computational integral imaging," *Opt. Lett.*, vol. 31, no. 8, pp. 1106–1108, Apr. 2006.

[13] B. G. Lee and D. H. Shin, "Enhanced computational integral imaging system for partially occluded 3D objects using occlusion removal technique and recursive PCA reconstruction," *Opt. Commun.*, vol. 283, no. 10, pp. 2084–2091, May 2010.

[14] S. Yeom, B. Javidi, and E. Watson, "Photon counting passive 3D image sensing for automatic target recognition," *Opt. Exp.*, vol. 13, no. 23, pp. 9310–9330, Nov. 2005.

[15] B. Tavakoli, B. Javidi, and E. Watson, "Three dimensional visualization by photon counting computational integral imaging," *Opt. Exp.*, vol. 16, no. 7, pp. 4426–4436, Mar. 2008.

[16] J. Jung, M. Cho, D. K. Dey, and B. Javidi, "Three-dimensional photon counting integral imaging using Bayesian estimation," *Opt. Lett.*, vol. 35, no. 11, pp. 1825–1827, Jun. 2010.

[17] I. Moon and B. Javidi, "Three dimensional imaging and recognition using truncated photon counting model and parametric maximum likelihood estimator," *Opt. Exp.*, vol. 17, no. 18, pp. 15 709–15 715, Aug. 2009.

[18] I. Moon and B. Javidi, "Three-dimensional recognition of photon-starved events using computational integral imaging and statistical sampling," *Opt. Lett.*, vol. 34, no. 6, pp. 731–733, Mar. 2009.

[19] M. DaneshPanah, B. Javidi, and E. A. Watson, "Three dimensional object recognition with photon counting imagery in the presence of noise," *Opt. Exp.*, vol. 18, no. 25, pp. 26 450–26 460, Dec. 2010.

[20] D. Aloni, A. Stern, and B. Javidi, "Three-dimensional photon counting integral imaging reconstruction using penalized maximum likelihood expectation maximization," *Opt. Exp.*, vol. 19, no. 20, pp. 19 681–19 687, Sep. 2011.

[21] C. M. Do and B. Javidi, "Three-dimensional object recognition with multiview photon-counting sensing and imaging," *IEEE Photon. J.*, vol. 1, no. 1, pp. 9–20, Jun. 2009.

[22] S. H. Hong, J. S. Jang, and B. Javidi, "Three-dimensional volumetric object reconstruction using computational integral imaging," *Opt. Exp.*, vol. 12, no. 3, pp. 483–491, Feb. 2004.

[23] D. Unholtz, W. Semmler, O. Dössel, and J. Peter, "Image formation with a microlens-based optical detector: A three-dimensional mapping approach," *Appl. Opt.*, vol. 48, no. 10, pp. D273–D279, Apr. 2009.

[24] L. Cao and J. Peter, "Iterative reconstruction of projection images from a microlens-based optical detector," *Opt. Exp.*, vol. 19, no. 13, pp. 11 932–11 943, Jun. 2011.

[25] A. Stern and B. Javidi, "Random projections imaging with extended space-bandwidth product," *J. Display Technol.*, vol. 3, no. 3, pp. 315–320, Sep. 2007.

[26] A. Stern and Y. Rivenson, "Compressive sensing techniques in holography," in *Proc. Inf. Opt.*, Jun. 2011, DOI:10.1109/WIO.2011.5981451.

[27] R. M. Willett, R. F. Marcia, and J. M. Nichols, "Compressed sensing for practical optical imaging systems: A tutorial," *Opt. Eng.*, vol. 50, no. 7, p. 072 601, Jul. 2011.
[28] R. M. Lewitt and S. Matej, "Overview of methods for image reconstruction from projections in emission computed tomography," *Proc. IEEE*, vol. 91, no. 10, pp. 1588–1611, Oct. 2003.
[29] N. Dey, L. Blanc-Feraud, C. Zimmer, P. Roux, Z. Kam, J. C. Olivo-Marin, and J. Zerubia, "Richardson–Lucy algorithm with total variation regularization for 3D confocal microscope deconvolution," *Microsc. Res. Tech.*, vol. 69, no. 4, pp. 260–266, 2006.
[30] M. Bertero, P. Boccacci, G. Desidera, and G. Vicidomini, "Image deblurring with Poisson data: From cells to galaxies," *Inv. Probl.*, vol. 25, no. 12, p. 123 006, Dec. 2009.
[31] V. Panin, G. Zeng, and G. Gullberg, "Total variation regulated EM algorithm [SPECT reconstruction]," *IEEE Trans. Nucl. Sci.*, vol. 46, no. 6, pp. 2202–2210, Dec. 1999.